Acoustical Characterization of Micro-Bubbles Clouds by Attenuation and Velocity Spectroscopy

Lilian D'Hondt[1,2]*, Matthieu Cavaro[1], Cédric Payan[2], Serge Mensah[2]
[1] CEA Cadarache – DEN/DTN/STCP/LIET – Bat 202 – 13108 St Paul lez Durance - France
[2] Aix Marseille Univ, LMA UPR CNRS 7051, Marseille, France

Abstract

In 4th generation nuclear reactors cooled with liquid sodium, argon micro-bubbles are present in the primary opaque sodium. Acoustic control methods are chosen for operating inspections but this bubble presence greatly affects the acoustical properties of the medium. It is therefore required to characterize the micro-bubble cloud, i.e. to provide the volume fraction and the bubble size distribution. Safety authorities requires the proposed method to be robust and applicable with as few assumptions (about the bubble populations) as possible. The objective of this study is to evaluate the performance of spectroscopic methods based on celerity and attenuation in the presence of bubbles whose size and surface contributions are very different. Two methods of evaluating the histogram and the void fraction are compared. The first is based on the inversion of the integral equation of the complex wave number derived by Commander and Prosperetti[1]. The second, which assumes the populations to have log-normal or sums of Gaussian distributions, performs an adjustment of the distribution's parameters to fit spectral attenuation and celerity curves measurements. These methods are compared with experimental data obtained using ACWABUL facilities at CEA Cadarache.

1 Introduction

With increasing energy consumption around the world, the energy production will be an issue in the next decades. That's why the Generation IV International Forum has been settle *"to carry out the research and development needed to establish the feasibility and performance capabilities of the next generation nuclear energy systems."*[1]

Within this program, France has made the choice to concentrate its research on the Sodium Fast Reactors (SFR). Indeed, several SFR prototypes has already been build in France: Rapsodie (1967 - 1983), Phenix (1974 - 2009) and Superphenix (1984 - 1997). These reactors have demonstrated the feasibility of this technology to answer the gen-4 requirements, witch should be reach within the development of ASTRID[2]. However, some issues must be studied for the operation of ASTRID. One of these is the characterization of the micro-bubble cloud in the primary circuit.

Due to the Argon gas plenum, a normal and continuous micro-bubble cloud in the primary circuit exists. These bubbles mainly come from the dissolution of gas in the hot sodium, and then nucleation within the colder sodium. Consequently, there is a risk of accumulation and release of large gas pockets which could affect the core reactivity. Moreover, micro-bubbles have an impact on boiling, cavitation and the liquid sodium's acoustic properties are deeply affected. Here, characterization means at least obtaining the void fraction $\tau = \frac{gas\ volume}{total\ volume}$ and, if possible, the bubble radius distribution. Today, the characterization of bubbly liquids is a topic of interest in several domains: oceanography; medicine, with the studies on contrast agents and decompression sickness prevention[2]; industry, for example the studies on cavitation[3]... So, the framework of this article is not restricted to nuclear purposes. The interest in bubbly liquids characterization is not new and comes with Medwin [4, 5] in 1970 in order to understand the bubble's population on top of the oceans. He used an analytic expression to get the bubble radius distribution from attenuation measurements. Only the resonant bubbles were taken into account. This method has been improved by Caruthers and Elmore [6, 7] who used an interative procedure to reduce the impact of the approximations made by Medwin. However, Commander and Moritz shown [8] that the non-resonant bubbles should be taken into accounts for better results. This implies the utilization of numeric methods to solve the integral equation that links the bubble distribution to the acoustic properties. The first numeric method was given by Commander and Moritz [9] and it has mainly been improved by the team of the Dynaflow laboratory. Duraiswami and al. [10–14] improvement mainly arise from the use of velocity measurement in the inversion process. Leighton [15] also used this

*lilian.d'hondt@cea.fr
[1] $https://www.gen-4.org/gif/jcms/c_9260/public$
[2] Advanced Sodium Technological Reactor for Industrial Demonstration

method and gave a way to determine the regularization parameter required for the inversion process.

The aim of this paper is to present a method based on the spectroscopic measurements of attenuation and velocity. In the first section, the different equations for wave propagation in a bubbly liquid will be described. The impact of the bubble size distribution is shown. In a second part, two ways of obtaining the bubble size distribution will be described: the first one is by Tikhonov regularization and the other by fitting procedures. Finally, both approaches are employed and validated using acoustical and optical experimental data. However, the acoustic characteristic of this two medium are similar so a valid method in water should be efficient in liquid sodium provided adequate sodium-proof transducers are available.

2 Wave propagation in bubbly liquids

In this section, the specificities of a pressure wave propagation in a bubbly liquid are presented. When a bubble is subjected to a pressure wave, it will oscillate accordingly to the Keller-Miksis equation [16] :

$$\begin{cases} \left(1-\frac{\dot{R}}{c}\right)R\ddot{R}+\frac{3}{2}\dot{R}^2\left(1-\frac{\dot{R}}{3c}\right) \\ \qquad =\left(1+\frac{\dot{R}}{c}\right)\frac{p_B(t)}{\rho}+\frac{R}{\rho c}\dot{p_B}(t) \\ p_B(t)=\left(p_0+\frac{2\sigma}{R_0}-p_v\right)\left(\frac{R_0}{R}\right)^{3\kappa}-\frac{2\sigma}{R_0} \\ \qquad -\frac{4\mu}{R}\dot{R}+p_v-p_\infty(t) \end{cases} \quad (1)$$

where the different notation are described at the end of the article, and $p_\infty(t)$ is the sum of the hydrostatic pressure and the fluctuating acoustic pressure.

This equation is strongly non linear and so, even at relatively low pressure ($> 5kPa$), non linear effects can arise from the wave's propagation in a bubbly liquid. These non linear properties can be used to characterize bubble clouds [17, 18]. However, it is supposed here that the wave amplitude is sufficiently low so that the propagation is almost linear. Commander and Prosperetti[1] have obtained from the linearization of the equation (1) the expression of the complex wave number k_m associated to a bubble size distribution: $N(a) = (\textit{number of bubbles per volume unit with radius between } a \textit{ and } a+da)$:

$$k_m^2=\frac{\omega^2}{c^2}+4\pi\omega^2\int_0^\infty\frac{aN(a)}{\omega_0^2-\omega^2+2i\beta\omega}da \quad (2)$$

where $w_0(a)$ is the resonant pulsation of a bubble of radius a. Here,

$$w_0^2=\frac{p_0}{\rho a^2}\left(Re(\Phi)-\frac{2\sigma}{ap_0}\right) \quad (3)$$

where Φ is given by equation (27) in Commander and Prosperetti's article[1]. Φ quantifies the thermal effects that affect the bubble pulsation.

u and v are defined such as the complex velocity $c_m = \omega/k_m$ is given by :

$$\frac{c}{c_m}=u-iv \quad (4)$$

then, the attenuation A in dB/m and the phase velocity V in $m.s^{-1}$ are defined by:

$$A=20log(e)\left(\frac{\omega v}{c}\right) \quad (5)$$

$$V=\frac{c}{u} \quad (6)$$

Depending on the excitation frequency, attenuation and velocity exhibits different behaviors.

At low frequencies: When the excitation frequency is much lower than the resonance frequency of the larger bubble, the bubbly liquid can be approximated by a homogeneous medium[19] of density ρ_m and compressibility χ_m defined by :

$$\begin{cases} \rho_m=(1-\tau)\rho_l+\tau.\rho_g \\ \chi_m=(1-\tau)\chi_l+\tau.\chi_g \end{cases} \quad (7)$$

and because here:

$$\rho_l \gg \rho_g \text{ and } \chi_g \gg \chi_l \quad (8)$$

using the general expression for velocity:

$$c=\frac{1}{\sqrt{\rho\chi}} \quad (9)$$

we get:

$$\frac{1}{c_{Wood}^2}=\frac{\tau^2\kappa}{c_g^2}+\frac{(1-\tau^2)}{c_l^2}+\tau(1-\tau)\left(\frac{\rho_l}{p}+\rho_g\chi_l\right) \quad (10)$$

So, at low frequencies, there is a direct relationship between velocity c_{Wood} and void fraction τ. This is very convenient for void fraction measurement. However, this method faces some practical problems when used in experiments. First, if the size the larger bubble is unknown, it is challenging to make sure that the frequency used is low enough for equation (7) to be valid. For example, a 100 μm bubble have a resonant frequency around 30 kHz. Secondly, generating frequencies around few kilohertz can be difficult for conventional devices and reflections problem can arise when working in a tank. However, if these issues are solved, a void fraction as low as 10^{-6} can generate a 1% deviation of velocity in water, (15 $m.s^{-1}$ shift) (fig. 1).

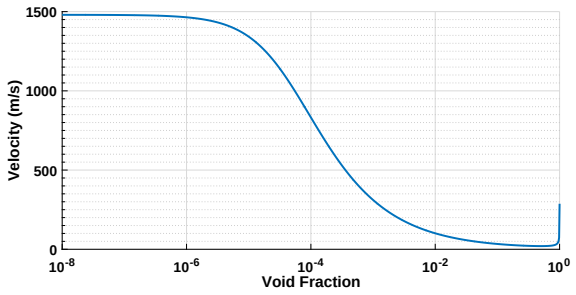

Figure 1: Velocity as a function of void fraction for air bubbles in water calculated using equation (10)

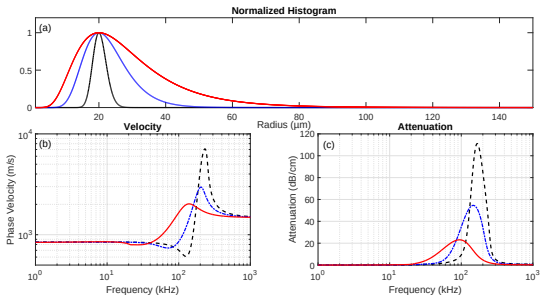

Figure 2: Impact of the bubble size distribution (a) on velocity (b) and attenuation (c). The distribution is log-normal (eq. (15)) with a scale parameter varying of 0.1 (black); 0.3 (blue) and 0.5 (red). $\tau = 10^{-4}$

Around the resonant frequencies and above: When the excitation frequency is around the bubbles resonances frequencies, the attenuation and velocity should be calculated using equations (5) and (6). Even if the void fraction remains the same, the dispersion curves are deeply affected by the bubble size distribution $N(a)$ (fig. 2). In this figure, the bubble size distribution is simulated using a log normal distribution. This distribution is representative of what is expected during the experiments. Here, only the impact of the distribution's shape is plotted. When the shape remains the same, but the void fraction increase, the frequencies impacted remains also almost the same. However attenuation and velocity variations are much larger. These behaviors are the basis of the interest for the bubble's characterization by acoustical means.

3 Inversion of spectroscopic measurements

As seen in the previous section, the dispersion curves can be strongly affected by any variation of the bubble size dispersion. In order to evaluate the bubble cloud's characteristics from spectral measurements, the inversion of equation (2) is required. In the following, regularization and fitting procedures are investigated.

3.1 Regularization procedure

By separating the complex wave number (equation (2)) into real and imaginary parts, Fredholm equations of the first kind [10] are obtained:

$$\alpha(f) = \int_{R_{\min}}^{R_{\max}} k(f,a)N(a)da \tag{11}$$

where α represent the attenuation and velocity measurements; $R_{\min} \equiv 0$ and $R_{\max}$ are the extremum radii of the bubble cloud. An erroneous choice could deeply affect the result of the inversion (as shown later in fig. 10). $k(f,a)$ is the kernel coming from the separation into real and imaginary part of equation (2) [10]. When only attenuation is measured, $k(f,a)$ is proportional to the extinction cross section [8].

Discretization of the equation (11) is performed to solve:

$$KN = \alpha \tag{12}$$

where α is now the vector of measurements: $\alpha_i = \alpha(f_i)$; K is the integration matrix and N is now the histogram of bubble size distribution.

However, the matrix K is badly conditioned, its singular values are very small, and so, any measurement error in α could result in large mistakes in N. Thus, equation (12) must be solved by a regularization procedure, here the Tikhonov regularization[20] is employed. This procedure consists in solving:

$$\min_N \left(\|KN - \alpha\|^2 + \lambda^2 \|N\|^2 \right) \tag{13}$$

where λ is the regularization parameter.

The solution of equation (13) is:

$$N = (K^T K + \lambda I)^{-1} K^T \alpha \tag{14}$$

where I is the identity matrix and K^T is the transposed matrix of K.

Equation (13) is solved using a quadratic procedure (*quadprog* routine in Matlab) to constraint the solution N as:

- For any radius a, $N(a) \geqslant 0$
- $\tau < 1$ at least, but a more restrictive maximum void fraction can be used.
- Any other information of interest. For example, if the void fraction or if the maximum radius of the bubble cloud is known, this can be added to improve the solution.

The optimal regularization parameter is determined using the L-curve method[21] (fig. 3). This parametric curve represents the solution's norm versus the error's norm for different values of λ. For $\lambda \ll \lambda_{optimal}$, the solution's norm is large but the error $\|KN - \alpha\|$ is small and should not vary too much, whereas for $\lambda \gg \lambda_{optimal}$, the solution's norm is small and almost constant but the error will increase as λ increase. This

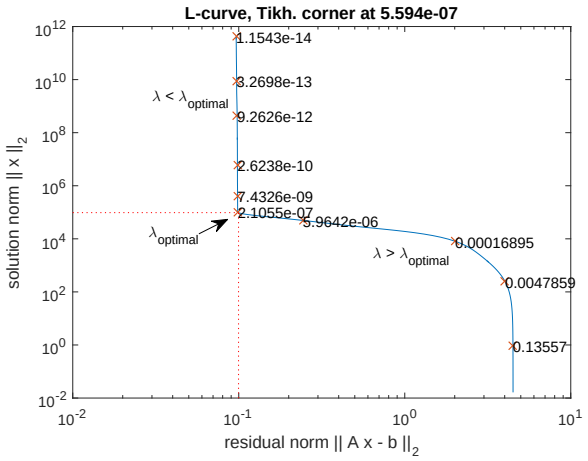

Figure 3: Example of a L-curve used for the determination of the optimal regularization parameter. Matlab script written by Hansen [22]

behavior explain the "L" shape of this curve (fig. 3). The optimal choice for the regularization parameter is then at the corner of the "L".

The impact of the regularization parameter's choice is shown in figure 4. From an arbitrary distribution (here log-normal), the dispersion curves are calculated using equations (5) and (6). A normally distributed random noise is added to these data to simulate experimental conditions. Even using the optimal regularization parameter, it remains some oscillations (fig. 4b). A larger λ could be used to suppress the oscillations, but it also underestimates the number of small bubbles (fig. 4c). This is why, the results are smoothed after inversion (blues curves on figure 4).

In practical applications, ultrasonic transducers present a finite bandwidth usually limited to $\pm 50\%$ of the central frequency. Several transducers can be used to over the entire frequency range, but as explained before, it can be challenging to employ frequencies low enough to cover the range of interest. In fig. 5, the impact of the total bandwidth is shown. In the first line, the measurement vector α is plotted versus frequency. The black curve is the theoretical α, the red stars show the measurements points and the dashed blue curve is the data calculated from the recovered histogram. When enough frequencies around the resonances frequencies are used, the results are satisfactory (fig. 5a and 5c). But, as we increase the minimum frequency of the working spectral interval, the result deteriorates. In fig. 5c, even if the shape of the recovered distribution is good, due to the high radii population ($[150 - 250m]$), the void fraction is wrong ($tau_{inv} = 2.10^{-4}$ vs $tau_{input} = 7.7e{-}6$). Moreover, the optimal regularization parameter should be $\ll 1$. So, in fig. 4c, the fact that $\lambda = 0.03$ indicates something is wrong.

Under proper bandwith conditions, this procedure provides satisfactory results, even with noisy data.

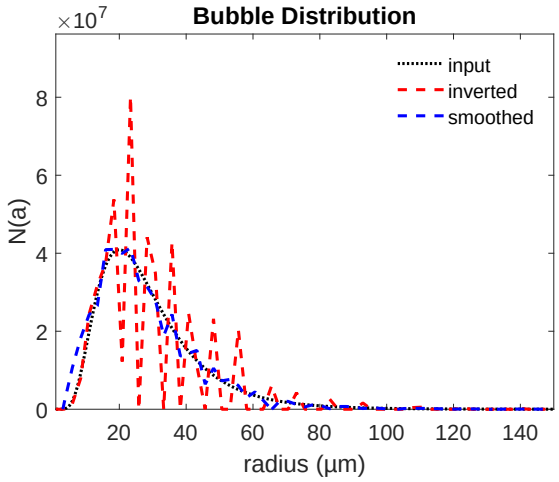

(a) $\lambda = 0$

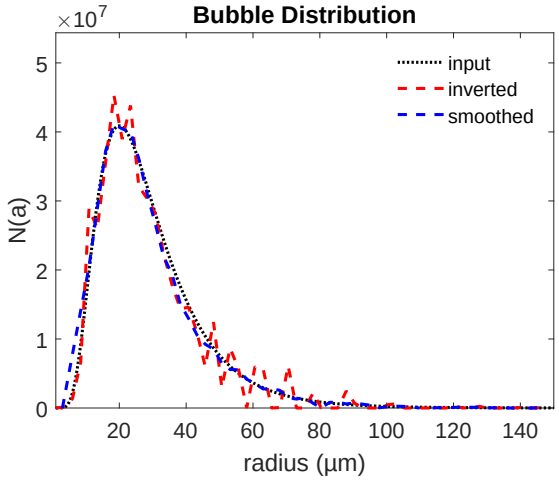

(b) $\lambda = \lambda_{optimal}$

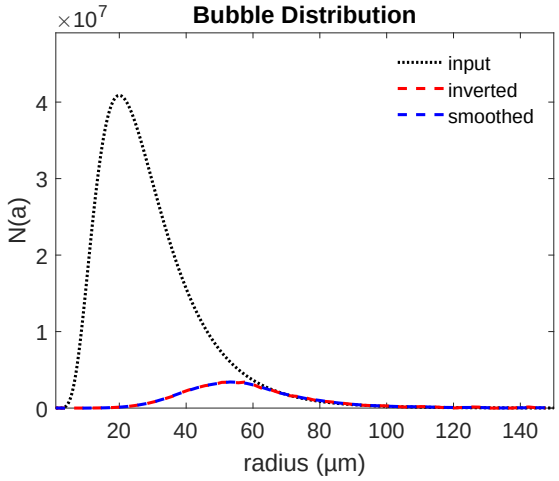

(c) $\lambda \gg \lambda_{optimal}$

Figure 4: Impact of the regularization parameter on the estimation of the bubble size distribution $N(a)$. Dotted black curve: input distribution. Red dashed curve: result of Tikhonov regularization. Blue dashed curve: smoothed curve

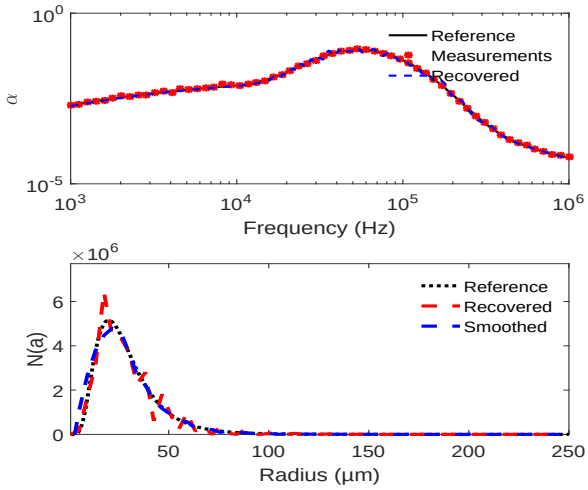

(a) Large bandwidth: $1kHz \leq f \leq 1Mhz$ $\lambda = 1.10^{-5}$ $\tau_{inv} = 7,3.10^{-6}$

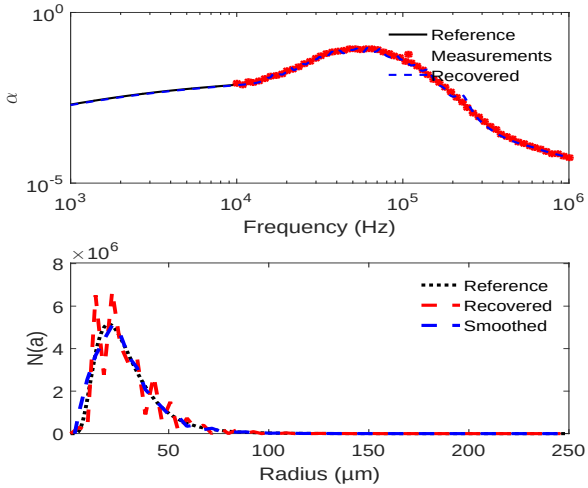

(b) Medium bandwidth: $10kHz \leq f \leq 1Mhz$ $\lambda = 2.10^{-5}$ $\tau_{inv} = 7,3.10^{-6}$

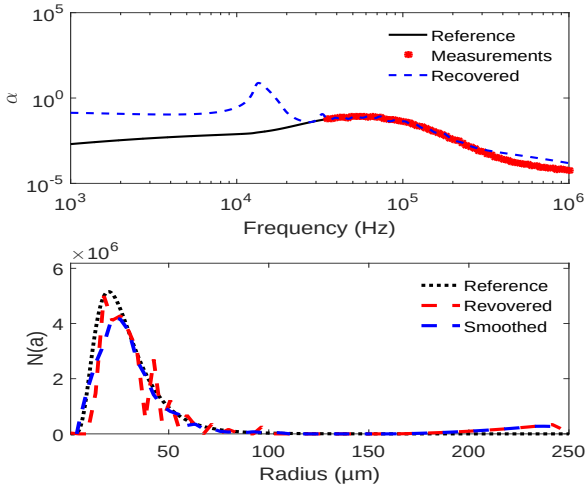

(c) Narrow bandwidth: $30kHz \leq f \leq 1Mhz$ $\lambda = 0.03$ $\tau_{inv} = 2.10^{-4}$

Figure 5: Impact of the measurement bandwidth - $\tau_{input} = 7.7e-6$

However, some oscillations remains and this procedure is dependent in the choice of the optimal regularization parameter. To overcome these issues, an other procedure is examined in the next sub-section.

3.2 Fitting procedure

The bubble size distribution in experiments can often be approximated with common probability density functions such as the log-normal distribution [23]:

$$N(a) = C \times \frac{1}{\sigma\sqrt{2\pi}} \exp\left[-\frac{(\ln a - a_0)^2}{2\sigma^2}\right] \tag{15}$$

where here σ is a scale parameter and a_0 is the mean radius of the bubble size distribution. To be able to deal with more complex bubbles clouds, e.g. clouds with two distinct bubbles size, a sum of multiple Gaussian can also be used:

$$N(a) = \sum_i \left[C_i \times \frac{1}{\sigma_i\sqrt{2\pi}} \exp\left[-\frac{(a - a_{0i})^2}{2\sigma_i^2}\right]\right] \tag{16}$$

The correct parameters $(\sigma_i,\ a_{0i},\ C_i)$ are calculated by a least square procedure, that is find the set of coefficients $x = [\sigma_1, a_{01}, C_1, ..., \sigma_n, a_{0n}, C_n]$ that solves the problem:

$$\begin{aligned} &\min_x \left\| F(x,f) - \begin{bmatrix} A_{measur} \\ V_{measur} \end{bmatrix} \right\| \\ &\text{where :} \\ &F : (x,f) \longmapsto \begin{bmatrix} A_x(f) \\ V_x(f) \end{bmatrix} \end{aligned} \tag{17}$$

F is the function that takes the distribution parameters x and the frequency of measurement vector $f = [f_1, ..., f_M]$ and provides the attenuation and velocity calculated with equations (5) and (6). A_{measur} and V_{measur} are the vectors of attenuation and velocity measured at each frequency f_i. The same constraints as in equation (13) can be added in the optimization routine. An initial value x_0 is set to start the algorithm. If x_0 is too different from the solution, the optimization will not converge. This is the main drawback of this technique. However, the regularization step is no longer required with this method.

An example is plotted fig. 6. In this figure, 5 gaussian has been used to recover a distribution represented by a log normal distribution. The population is well recovered excepted in the lower radii. Indeed, the very small bubbles have a very week impact on attenuation as their void fraction contribution is very small. Also, this procedures allows using few measurements points. Moreover, fitting with the log-normal distribution is fast ($\approx 2s$) and gives good results when dealing with distributions close to log normal distributions.

To summarize, the Tikhnov regularization allows *a priori* the determination of bubble size distribution of any shape. However, it requires more data

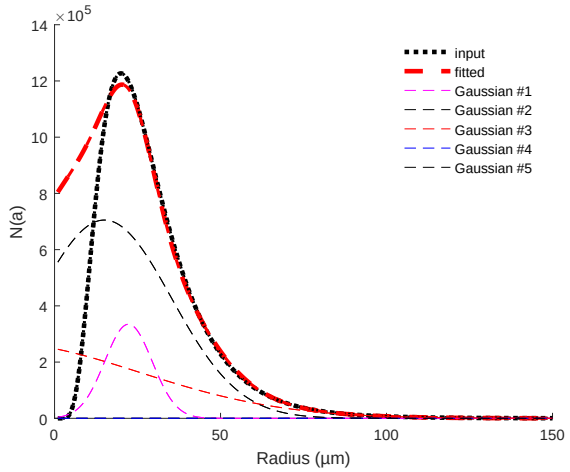

Figure 6: Result of the fitting procedures. The thin dashed lines are the different Gaussian witch constitute the solution

than the fitting procedure to be efficient and the results depends on the good choice of the regularization parameter λ because the L-curve can be ambiguous. To overcome these issues, the degrees of freedoms is reduced using the assumption of a solution as log-normal or in sum of Gaussian distribution. However, dealing with "complex" bubble size distributions, the sum of few Gaussian might not be sufficient to fully describe the bubble cloud. But this can be representative of the bubble size expected distribution in experiments and in the SFRs.

4 Experimental results

The efficiency of the inversions processes detailed above is evaluated using experimental data acquired in the ACWABUL[3] bench at CEA Cadarache. A saturator over-saturates water in air. Then this over-saturated water cavitates in the different injectors located at the bottom of the tank, which generates stable air micro-bubbles.

To estimate the phase velocity and attenuation at every frequency of interest, transmission measurement are performed by sending two sets of M monochromatic 10-cycles bursts. To cover the entire frequency range of interest - from $10kHz$ to $400kHz$- a set of multiple transducer is used. The waveforms are generated using a function generator Tektronix AFG 3022B and the oscilloscope is a PicoScope 4824. Both these devices are piloted by a dedicated Matlab script to allow fast measurements. The transducers used are standard ultrasonic transducers.

The first set is sent in pure water. Each burst is compared to the ones transmitted in the bubbly liquid (fig. 7).

[3]Acoustic Characterization in WAter of microBUbbuLes

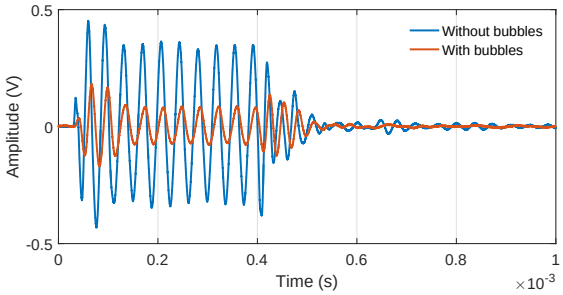

Figure 7: Example of bursts received. $f = 13kHz$

In figure 7, the effect of attenuation and velocity modification are clear. To estimate attenuation the root mean square amplitudes of the bursts (RMS) are compared. In the same way, to evaluate the velocity, the time shift Δt_{corr} between the bursts is determined by cross correlation.

$$\begin{aligned} A_{measur} &= 20 \log \left[\frac{RMS_m}{RMS_l} \right] \\ V_{measur} &= \frac{d}{\frac{d}{c_l} + \Delta t_{corr}} \end{aligned} \tag{18}$$

where d is the distance between the emitter and the receiver and Δt_{corr} is the time shift measured by correlation between the signals with and without bubbles.

To validate our results, an optical device is employed simultaneously. Several pictures of the clouds are taken during the experiments (fig. 8a). Then, a dedicated algorithm estimates the bubble size distribution (fig. 8b) and the void fraction. The void fraction estimation is achieved by estimating the blurring level on each bubble in order to estimate its distance from the focal plan of the camera. Then, a volume of measurement is delimited and the void fraction is estimated. This optical void fraction measurement relies on a correct calibration procedure and requires that the bubbles are all detected and properly measured. In practical, some bubbles may hide other ones and conversely, a dust for example can be treated as a bubble. Then, the optical measurement is local, whereas the volume scanned by acoustics is much larger. These can partially explain the bias between the void fractions measurement. In all case, the optical measurement of the void fraction provides an estimation of the true void fraction.

Spectroscopic measurements of attenuation and velocity are performed on the same bench. The optical device is also set inside the bubble clouds, as close as possible to the acoustic transducers. Both regularization and fitting methods run on the same acoustical data (fig. 9). However, due to the strong attenuation ($\simeq 80dB.m^{-1}$ at resonance), the velocity measurements where not exploitable. The is why the inversion is only performed on attenuation data.

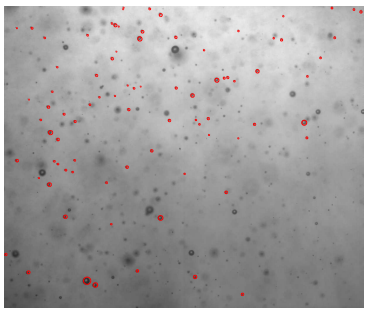

(a) One picture of the clouds and the bubbles detected. The void fraction is estimated to be around 1.4×10^{-4}

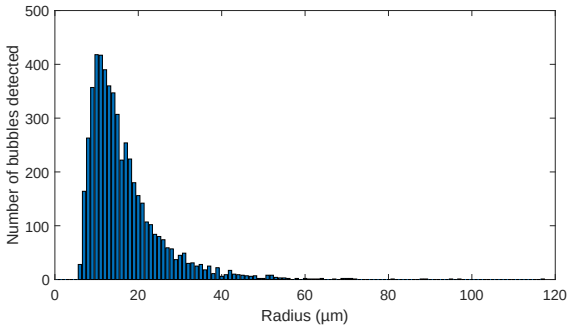

(b) Optical histogram obtained after treatment

Figure 8: A picture of the cloud and the histogram associated

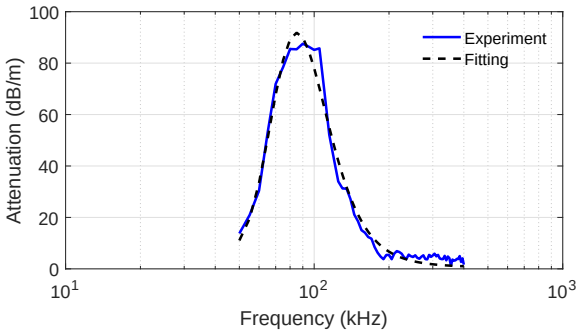

Figure 9: Experimental attenuation and attenuation obtained by fitting

For the Tikhonov regularization, the maximum integration radius $R_{\max}$ is chosen to produce better L-curve which is the one with the sharpest corner, and the straightest lines. For the L-curves depicted figure 10,the best is for $R_{\max} = 200\mu m$. This part of the procedures isn't automated as it allows some manual adjustments, for example it allows the selection of a better regularization parameter than the one predicted by the algorithm when the L-curve is ambiguous.

The full results are presented in figure 11. For better visibility, the various distribution obtained are normalized. Indeed, the Tikhonov procedure may give some big bubbles populations which scale down the

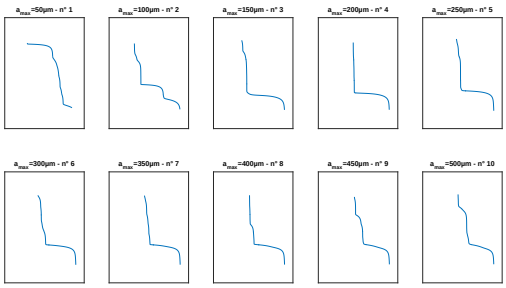

Figure 10: Several L-curves for different maximum radius of integration $R_{\max}$.

histogram without changing the void fraction. Indeed, the remaining oscillations have a strong impact on void fraction when they concern bigger bubbles. A fitting is also made on these data. The figure 9 shows that the measured attenuation and the fitted one correspond each other nicely.

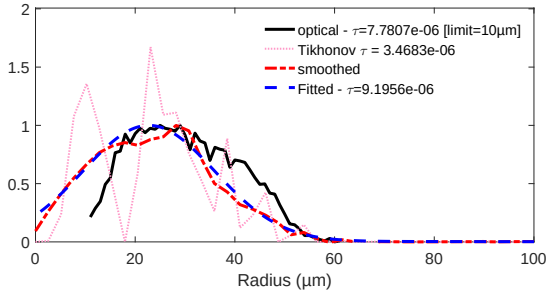

Figure 11: Experimental results. The distribution are normalized for better visibility.

The void fraction obtained by all the methods are of the same order of magnitude. The shape of the distributions are also similar. The remaining biases can be explained for different reasons. First, the lack of the velocity information can induce some discrepancies between the different curves. The optical device's resolution limits the histogram reconstruction to $10\mu m$, and confident values are certainly reached at about $20\mu m$. Then, the inversion is dependent on the propagation model used. Here, the model by Commander and Prosperetti is employed. And, as the authors showed, there are some discrepancies between the theoretical and experimental data, especially around the resonances frequencies. Despite these small disagreement , the overall distributions and void fraction are really close to each others, providing confidence on the procedures.

5 Conclusion

In order to provide the bubble size distribution (and the void fraction) from attenuation and velocity mea-

surements, a way to invert the complex wave number is proposed. Two methods based on Tikhonov regularization and fitting procedures are presented. The limits and performances of both methods are analyzed numerically and validated experimentally. It is shown that the Tikhonov regularization is efficient to characterize bubble clouds if a correct regularization parameter is chosen and enough data are provided. But it can be difficult to provide these latter. Indeed, the transducer have a limited bandwidth and the L-curve is sometimes ambiguous. So, an other method has been set up. The bubble size distribution is approximated as being log-normal or multi-Gaussian, as the bubble size distribution is expected to look like in ASTRID. Then, a fit of the experimental data is made. So, no regularization parameter is longer required and because there are less degree of freedom is than with the regularization procedure, less data are needed.

Future studies will aim at improving the experimental setup in order to be able to use the velocity in the inversion. Moreover, as the range of radii isn't known *a priori* for practical application in SFRs, the frequency range used is just a guess and it might not be sufficient. The addition of new data in the inversion, such as nonlinear parameters, are also currently considered to improve the reliability of these methods.

Symbols

- Subscript '$_0$' denote the initial or equilibrium value.
- Subscript '$_m$' denote the mixture value.
- Subscript '$_g$' denote the gas value.
- Subscript '$_l$' denote the pure liquid value.

Same symbol can be use for different meaning, but this should not raise any confusion in the equation.

Symbol	Name
ρ	Density
c	Velocity
c_{Wood}	Low Frequency Velocity
R	Bubble radius
σ	Surface tension constant
σ	scale parameter of the distribution law
p_v	Vapor pressure
κ	Polytropic constant
μ	Total viscosity [24]
β	Damping constant
A	Attenuation in bubbly liquid
V	Phase Velocity in bubbly liquid
τ	Void fraction
χ	Compressibility
λ	Regularization parameter

References

[1] K. Commander and A. Prosperetti, "Linear Pressure Waves in Bubbly Liquids - Comparison Between Theory and Experiments," *J. Acoust. Soc. Am.*, vol. 85, pp. 732–746, Feb. 1989. WOS:A1989T156000025.

[2] D. Fouan, Y. Achaoui, C. Payan, and S. Mensah, "Microbubble dynamics monitoring using a dual modulation method," *The Journal of the Acoustical Society of America*, vol. 137, pp. EL144–EL150, Feb. 2015.

[3] D. L. Miller, "Ultrasonic detection of resonant cavitation bubbles in a flow tube by their second-harmonic emissions," *Ultrasonics*, vol. 19, pp. 217–224, Sept. 1981.

[4] H. Medwin, "In situ acoustic measurements of bubble populations in coastal ocean waters," *J. Geophys. Res.*, vol. 75, pp. 599–611, Jan. 1970.

[5] H. Medwin, "Acoustical determinations of bubble-size spectra," *The Journal of the Acoustical Society of America*, vol. 62, pp. 1041–1044, Oct. 1977.

[6] J. W. Caruthers, P. A. Elmore, J. C. Novarini, and R. R. Goodman, "An iterative approach for approximating bubble distributions from attenuation measurements," *The Journal of the Acoustical Society of America*, vol. 106, pp. 185–189, July 1999.

[7] P. Elmore and J. Caruthers, "Higher order corrections to an iterative approach for approximating bubble distributions from attenuation measurements," *IEEE Journal of Oceanic Engineering*, vol. 28, pp. 117–120, Jan. 2003.

[8] K. Commander and E. Moritz, "Off-resonance contributions to acoustical bubble spectra," *The Journal of the Acoustical Society of America*, vol. 85, pp. 2665–2669, June 1989.

[9] K. Commander and E. Moritz, "Inferring Bubble Populations in the Ocean from Acoustic Measurements," in *OCEANS '89. Proceedings*, vol. 4, pp. 1181–1185, Sept. 1989.

[10] R. Duraiswami, "Bubble Density Measurement using an Inverse Acoustic Scattering Technique," *ASME*, vol. 153, pp. 67–73, 1993.

[11] R. Duraiswami, S. Prabhukumar, and G. L. Chahine, "Acoustic measurement of bubble size distributions: Theory and experiments," *The Journal of the Acoustical Society of America*, vol. 100, no. 4, p. 2804, 1996.

[12] R. Duraiswami, S. Prabhukumar, and G. L. Chahine, "Bubble counting using an inverse acoustic scattering method," *The Journal of the Acoustical Society of America*, vol. 104, pp. 2699–2717, Nov. 1998.

[13] X.-j. Wu and G. L. Chahine, "Development of an acoustic instrument for bubble size distribution measurement," *Journal of Hydrodynamics, Ser. B*, vol. 22, pp. 330–336, Oct. 2010.

[14] G. L. Chahine and K. M. Kalumuck, "Development of a Near Real-Time Instrument for Nuclei Measurement: The ABS Acoustic Bubble Spectrometer®," pp. 183–191, Jan. 2003.

[15] T. G. Leighton, S. D. Meers, and P. R. White, "Propagation through nonlinear time-dependent bubble clouds and the estimation of bubble populations from measured acoustic characteristics," *Proceedings of the Royal Society of London A: Mathematical, Physical and Engineering Sciences*, vol. 460, pp. 2521–2550, Sept. 2004.

[16] J. B. Keller and M. Miksis, "Bubble oscillations of large amplitude," *The Journal of the Acoustical Society of America*, vol. 68, pp. 628–633, Aug. 1980.

[17] M. Cavaro, C. Payan, S. Mensah, J. Moysan, and J.-P. Jeannot, "Linear and nonlinear resonant acoustic spectroscopy of micro bubble clouds," *Proceedings of Meetings on Acoustics*, vol. 16, p. 045003, Oct. 2012.

[18] M. Cavaro and C. Payan, "Microbubble histogram reconstruction by nonlinear frequency mixing," *Proceedings of Meetings on Acoustics*, vol. 19, p. 030111, June 2013.

[19] A. Wood, *A Textbook of Sound*. New York: Macmillian, 1930.

[20] D. Calvetti, S. Morigi, L. Reichel, and F. Sgallari, "Tikhonov regularization and the L-curve for large discrete ill-posed problems," *Journal of Computational and Applied Mathematics*, vol. 123, pp. 423–446, Nov. 2000.

[21] P. C. Hansen, "The L-Curve and its Use in the Numerical Treatment of Inverse Problems," in *Computational Inverse Problems in Electrocardiology, ed. P. Johnston, Advances in Computational Bioengineering*, pp. 119–142, WIT Press, 2000.

[22] P. C. Hansen, "REGULARIZATION TOOLS: A Matlab package for analysis and solution of discrete ill-posed problems," *Numer Algor*, vol. 6, no. 1, pp. 1–35, 1994.

[23] E. Verboven, E. D'Agostino, J. D'hooge, H. Pfeiffer, O. Bou Matar, and K. Van Den Abeele, "The Nonlinear Coefficient Dispersion of Ultrasound Contrast Agents and the Challenges of Current Microbubble Oscillation Models," (Singapore), 2013.

[24] M. J. Holmes, N. G. Parker, and M. J. W. Povey, "Temperature dependence of bulk viscosity in water using acoustic spectroscopy," *J. Phys.: Conf. Ser.*, vol. 269, no. 1, p. 012011, 2011. bibtex: holmes_temperature_2011.